A pH-Tunable Nanofluidic Diode with a Broad Range of Rectifying Properties

Mubarak Ali,[†,*] Patricio Ramirez,[‡] Salvador Mafé,[§] Reinhard Neumann,[∥] and Wolfgang Ensinger[†]

[†]Technische Universität Darmstadt, Fachbereich Material-u. Geowissenschaften, Fachgebiet Chemische Analytik, Petersenstrasse 23, D-64287 Darmstadt, Germany, [‡]Depto. de Física Aplicada, Universidad Politécnica de Valencia, E-46022 Valencia, Spain, [§]Dept. de Física de la Terra i Termodinàmica, Universitat de València, E-46100 Burjassot, Spain, and [∥]GSI Helmholtzzentrum für Schwerionenforschung GmbH, Planckstr. 1, D-64291 Darmstadt, Germany

ABSTRACT The use of fixed charge nanopores in practical applications requires tuning externally the electrostatic interaction between the charged groups and the ionic permeants in order to allow integrating a variety of functions on the same nanostructure. We design, produce, and characterize, theoretically and experimentally, a single-track amphoteric nanopore functionalized with lysine and histidine chains whose positive and negative charges are very sensitive to the external pH. This nanofluidic diode with amphoteric chains attached to the pore surface allows for a broad set of rectification properties supported by a single nanodevice. A definite plus is to functionalize these groups on a conical nanopore with well-defined, controlled structural asymmetry which gives virtually every rectification characteristic that may be required in practical applications. Nanometer-scaled amphoteric pores are of general interest because of the potential applications in drug delivery systems, ion-exchange membranes for separation of biomacromolecules, antifouling materials with reduced molecular adsorption, and biochemical sensors.

KEYWORDS: nanofluidics · nanopore · surface functionalization · amphoteric diode · rectification properties · Poisson–Nernst–Planck equations

Nanopores, nanopipettes, and nanoelectrodes are based on a new generation of devices designed for single-molecule sensing, molecular separation, and energy storage.[1−11] In particular, nanopores with fixed charges provide ionic selectivity and sensing, exploiting the fact that the internal pore volume is not much larger than the ionic analyte size.[9,12,13] The pore does not act simply as a mechanical filter because it displays also ionic selectivity due to the electrical charges attached to the surface. These charges favor the passage of counterions (ions with charge opposite to that of the pore) but hinder the passage of co-ions (ions with charge of the same sign as the pore).[1,14] The ionic selectivity is high when the surface potential is high and the radius of the pore is decreased down to the Debye length of the electrolyte, which is usually on the nanometer scale.[1,14,15]

The functionalization of chemical groups on the pore surface allows controlling the transport through the nanopore, and a variety of different substrate-specific methods aimed at modifying the nanopore surface have been reported (see ref 16 and references therein). The use of fixed charge nanopores in practical applications may require tuning externally the electrostatic interaction between the surface charge groups and the ionic permeants. This would allow integrating a variety of functions on the same nanostructure, as is the case of biological membranes where both positive (amino) and negative (carboxylic) fixed charge groups coexist in the same ion channel.[17] However, the fact is that the external control of the fixed charges is severely limited in most cases. In particular, no charge reversal is possible, except for the very specific case of gold-coated nanotubule membranes[18,19] where the application of an electric potential to the internal metallic surface of the pores allows implementing cation- and anion-exchange properties on a unique separation device. It constitutes a significant innovation to design, produce, and characterize, theoretically and experimentally, a single-track amphoteric nanopore containing both positively and negatively fixed charge groups whose properties are very sensitive to the external pH. In fact, previous work with amphoteric cross-linked polymer networks has been carried out mainly on the macroscopic scale (two well-known examples are hydrogels[20,21] and porous membranes).[22−24] Nanometer-scaled amphoteric pores are of general interest because of their potential applications in drug delivery systems, ion-exchange membranes for separation of biomacromolecules, antifouling materials with reduced molecular adsorption, and biochemical sensors.

*Address correspondence to m.ali@gsi.de.

Received for review January 15, 2009 and accepted February 09, 2009.

Published online February 17, 2009.
10.1021/nn900039f CCC: $40.75

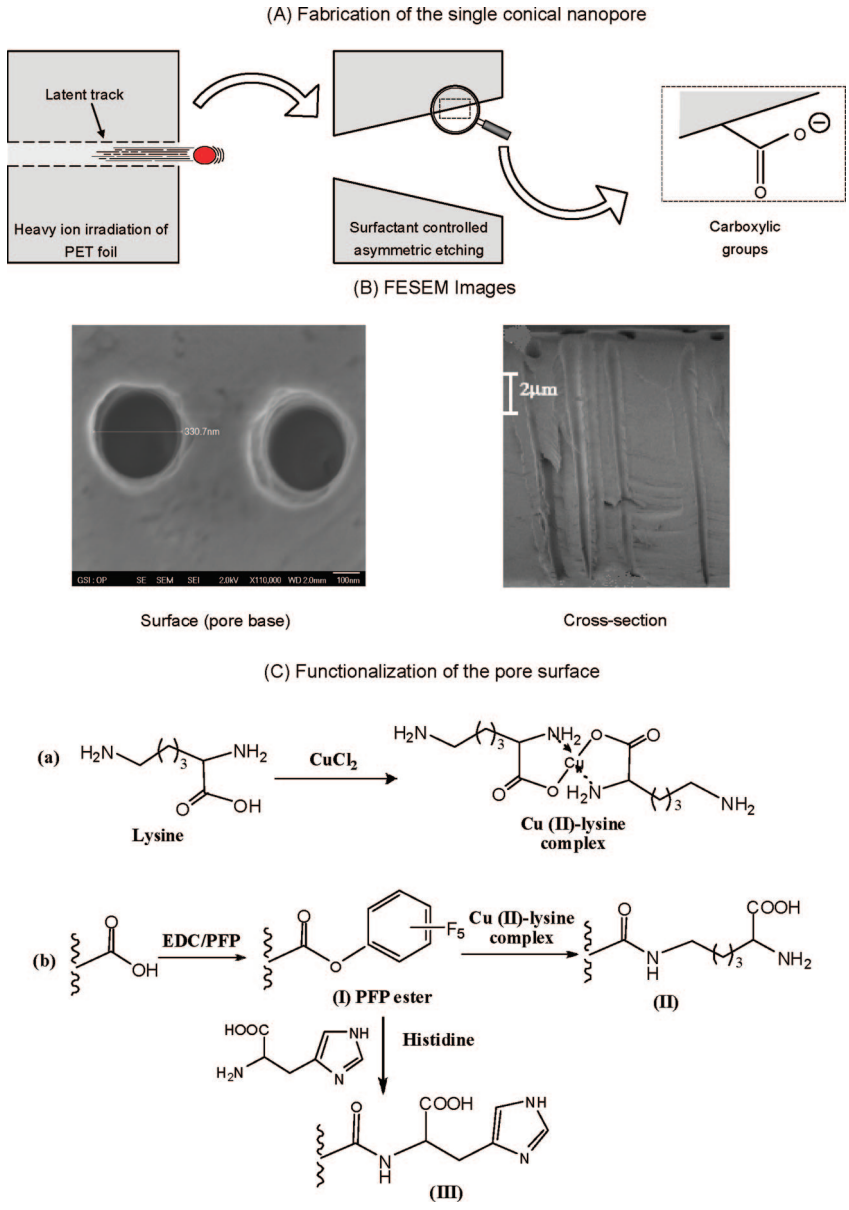

Figure 1. (A) Formation of the single conical nanopore after irradiation of the polymer foil with heavy ions and etching (see Materials and Methods). (B) FESEM (surface and cross section) images of a polymer foil containing 10^8 cm^{-2} nanopores approximately. (C) Functionalization of the pore surface with L-lysine and L-histidine.

Nanofluidic diodes based on asymmetric nanopores[25−28] and bipolar transistors[29,30] have recently been demonstrated. We go a step further here and demonstrate a nanofluidic diode with amphoteric chains (lysine or histidine) functionalized on the pore surface. This permits a broad set of rectification properties using the same nanodevice by changing simply the pH values in the external solutions. A definite plus is to functionalize the amphoteric chains on a conical nanopore with well-defined, controlled structural asymmetry because this gives unique selectivity and rectification properties. Conical nanopores have a small-diameter opening (tip), usually in the range of 1−10 nm.[1,12−14,31−34] Selectivity and rectification are dictated by the tip because it is in this narrow, nanometer-sized region where the influence of the radial electrical double layer and the major part of the applied axial voltage drop act together to determine the final device performance.[14,34] We demonstrate also that the intrinsic (geometric and electrostatic) asymmetries of the device permit one to obtain virtually every rectification characteristic that may be required in practical applications.

RESULTS AND DISCUSSION

Polymeric films with single conical nanopores, incorporating L-lysine or L-histidine as amphoteric chains, were obtained following the procedure described in the Materials and Methods. During the process of (asymmetric) track-etching in a polymer membrane, the carboxylic groups were generated on the pore surface (Figure 1A). The field emission scanning electron microscopy (FESEM) images (Figure 1B) show the surface (pore base) and fracture of the resulting conical nanopores obtained in a polymer foil containing 10^8 nanopores/cm^2, approximately. The lysine and histidine chains were attached onto these carboxylic groups according to the reaction schemes of Figure 1C (see also Materials and Methods). The selective functionalization of lysine with surface carboxylic groups was accomplished by blocking the amino group and carboxylic group bonded to the α-carbon with Cu^{2+} ion to form a copper−chelate complex, leaving an unprotected ε-amino group. The free ε-amino−terminator (−NH_2) of the copper(II)−lysine complex is covalently coupled with the carboxylic group originated during track-etching.[35] In order to break the complex, EDTA was used because it has a strong affinity to copper compared with amino acid (lysine) and forms a water-soluble copper chelate.[36] The resulting chain displays two ionizable residues: one α-carboxylic group (pK_a = 2.2)[37] and one α-amino group (pK_a = 9.0).[37] Histidine contains an imidazole ring at the terminus of its side chain along with amino (−NH_2) and carboxylic (−COOH) groups bounded to α-carbon. The histidine was functionalized on the channel surface through the covalent bond between amino and activated carboxylic groups. The imidazole side chain ring is protonated at slightly acidic pH values (pK_a = 6.7−7.1).[38]

Figure 2 shows the effect of pH on the *I*−*V* curves of an amphoteric nanopore functionalized with lysine. At low pH values (left), the ionized amino groups

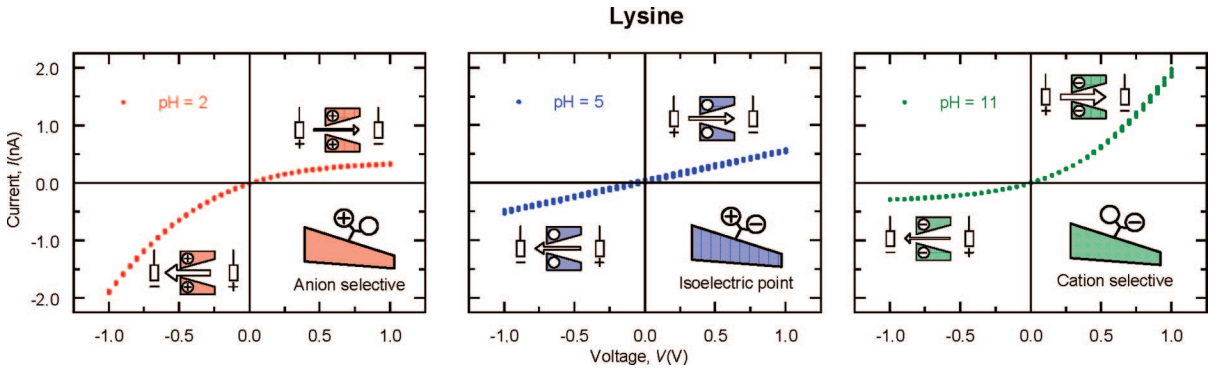

Figure 2. Current voltage curves of the amphoteric (lysine) nanopore at pH = 2 (left), pH = 5 (center), and pH = 11 (right).

($-NH_3^+$) are positively charged due to protonation, while the protonated carboxylic groups ($-COOH$) are neutral. The nanopore is then selective to anions and shows the rectification properties characteristic of conical pores with positive fixed charges:[25,39] a high conducting ("on") state for $V < 0$ and a low conducting ("off") state for $V > 0$. Conversely, at high pH values (right), the deprotonated amino groups ($-NH_2$) are in neutral form, while the carboxylic groups ($-COO^-$) are ionized. The net pore fixed charge is then negative, and the nanopore is now selective to cations. The nanopore "on" and "off" states appear at $V > 0$ and $V < 0$, respectively. The transition between these two rectification regimes occurs at pH = 5 (center), which is close to the isoelectric point pI = 5.6 of the lysine chain attached to the pore surface calculated from the pK_a values of the α-carboxylic and the α-amino groups.[37] At this pH value, the α-carboxylic and the α-amino groups are charged, but the nanopore net charge is zero, and the $I-V$ curve shows a linear, ohmic behavior. The reversal of the nanopore selectivity with increasing pH is further confirmed by independent reversal potential measurements giving −10 mV (pH = 2), 0 mV (pH = 5), and +32 mV (pH = 11) for an external solution concentration ratio of 0.1 M/0.01 M (0.1 M KCl on the base side and 0.01 M KCl on the tip side of the pore).

The $I-V$ curves obtained with the conical nanopore modified with histidine (not shown) display characteristics similar to those of Figure 2. At pH = 2.0, the protonated carboxylic is neutral while the ionized imidazole group provides a net positive charge. The isoelectric point is now pI = 4.2, leading to the linear $I-V$ curve. The channel starts rectifying again at pH values above the isoelectric point because of the ionized carboxylic groups. At pH > 7.0, the unprotonated imidazole group (pK_a = 6.7−7.1) becomes neutral, and only the carboxylic groups are responsible for the negatively charged channel surface.

Figure 3 shows the effect of changing the pH on the $I-V$ curves of the nanopore functionalized with lysine (Figure 3A) and histidine (Figure 3B). The curves obtained with the two nanopores give a progressive change of the nanopore charge (and then of the current) between the two experimental limits of low pH (most α-amino groups are positively charged) and high pH (most α-carboxylic groups are negatively charged). Comparison of the curves for the two samples shows higher currents for the lysine nanopore than for the histidine nanopore. The curves for pH = 2 and 11 are almost perfectly symmetrical in the case of lysine. However, in the case of histidine, the electric currents are slightly higher for pH = 10 than for pH = 2. This could be ascribed tentatively to two effects: first, substitution of the carboxylic groups by the histidine chains could be less effective for histidine than for lysine; sec-

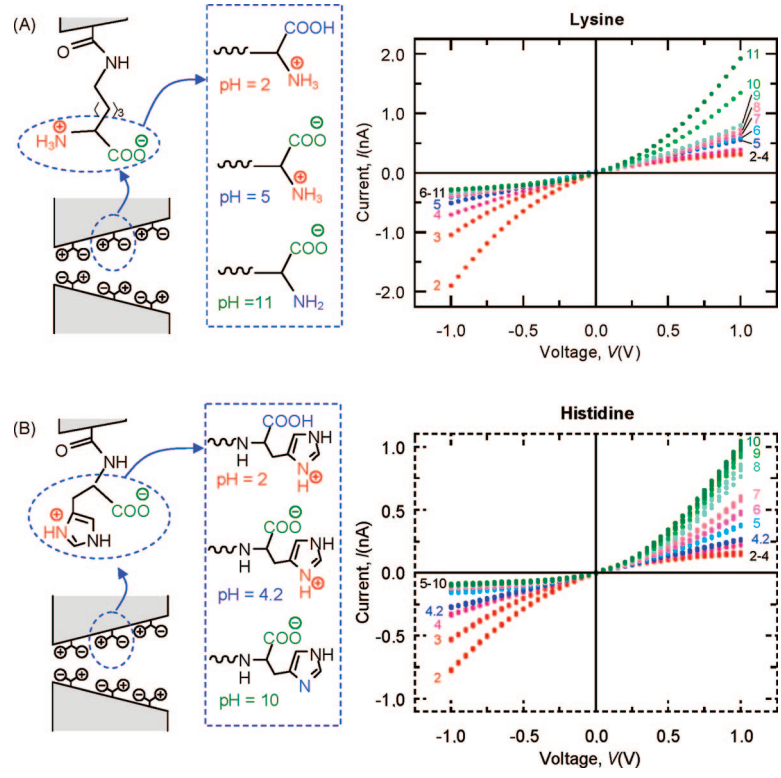

Figure 3. (A) Effect of pH on the $I-V$ curves of the amphoteric (lysine) nanopore. (B) Effect of pH on the $I-V$ curves of the amphoteric (histidine) nanopore. The numbers in the curves correspond to the pH values.

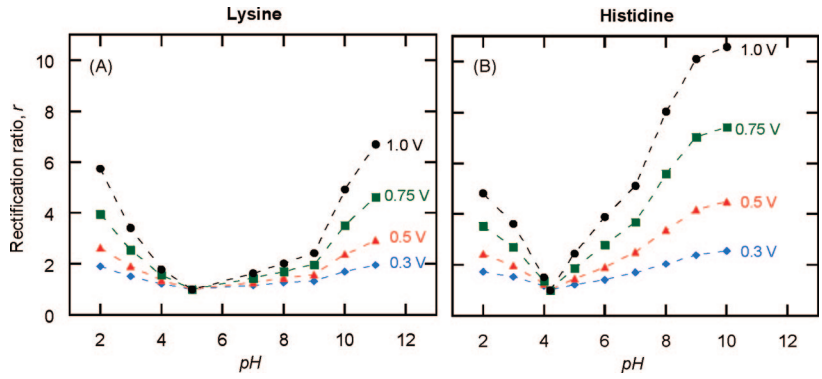

Figure 4. (A) Rectification ratio *versus* pH at different applied voltages (lysine). (B) Rectification ratio *versus* pH at different applied voltages (histidine). The numbers in the curves correspond to the on/off voltages for the rectification ratio.

ond, the interactions between the carboxylic and amino groups are likely to be different for lysine and histidine because of spatial constraints. These two effects may yield a net charge lower (in absolute value) at pH = 2 than that attained at pH = 10.

Figure 4 shows the rectification ratio, *r*, defined as the absolute value of the current ratio *I*(on state)/*I*(off state) at a given voltage, *versus* the pH value of the external solutions. As in the case of the *I*−*V* curves in Figure 3, the rectification characteristics are slightly different for the two nanopores. The experiments indicate again a symmetry between the points measured at pH = 2 and 11 in the case of lysine (Figure 4A). However, the nanopore functionalized with histidine (Figure 4B) shows an *r* value significantly higher for pH = 10 than that for pH = 2, probably because of the reasons mentioned for the *I*−*V* curves of Figure 3. The results obtained with the two nanopores reveal that the rectification ratio can be reversed simply by changing the pH of the solutions. Therefore, the amphoteric nanopore shows tunable ionic selectivity and rectification characteristics. In particular, a number of functions including diode rectification in nanofluidic circuits,[9,25,27,28] sensing,[7,12,13,40] separation,[18,19] electrophoretic capture/release of a charged species,[2] and ion pumping against an external concentration gradient,[1] could now be implemented on the basis of the nanostructure characteristics demonstrated in Figures 3 and 4.

The above experimental results can now be described theoretically in terms of a continuous model based on the Poisson and Nernst−Planck (PNP) equations[39]

$$\nabla^2\phi = \frac{F}{\varepsilon}(c_{Cl^-} - c_{K^+}) \quad (1)$$

$$\nabla\cdot\vec{J}_i = -\nabla\cdot[D_i(\nabla c_i + z_i c_i \nabla\phi)] = 0, \quad i = K^+, Cl^- \quad (2)$$

where $\vec{J}_i$, c_i, D_i, and z_i are the flux, the local concentration, the diffusion coefficient, and the charge number of ion i (i = K^+ and Cl^-), with ϕ and ε the local electric potential and the dielectric permittivity of the solution within the pore, respectively. Despite the nanometer scales involved in the problem, the fact is that most models of selectivity are still based on the classical continuum theories because these are relatively simple and predict correctly the qualitative trends of the problem.[1,2,14,15,26,34,41−46] Comparison between theory and experiment reveals that the agreement between the PNP theory and the experiments is also quantitative for the two nanopores (Figure 5A for lysine and 5B for histidine) and allows for the determination of the nanopore surface charge by using the following procedure. First, the radius of the wide pore opening is determined by FESEM (Figure 1B), using a polymer foil containing approximately 10^7 pores cm^{-2}, which was etched simultaneously with the sample containing the single pore under the same conditions. Second, the radius of the pore tip is calculated from the (linear) fitting of the *I*−*V* curve at the respective isoelectric points (Figure 2, center). Once the pore radii have

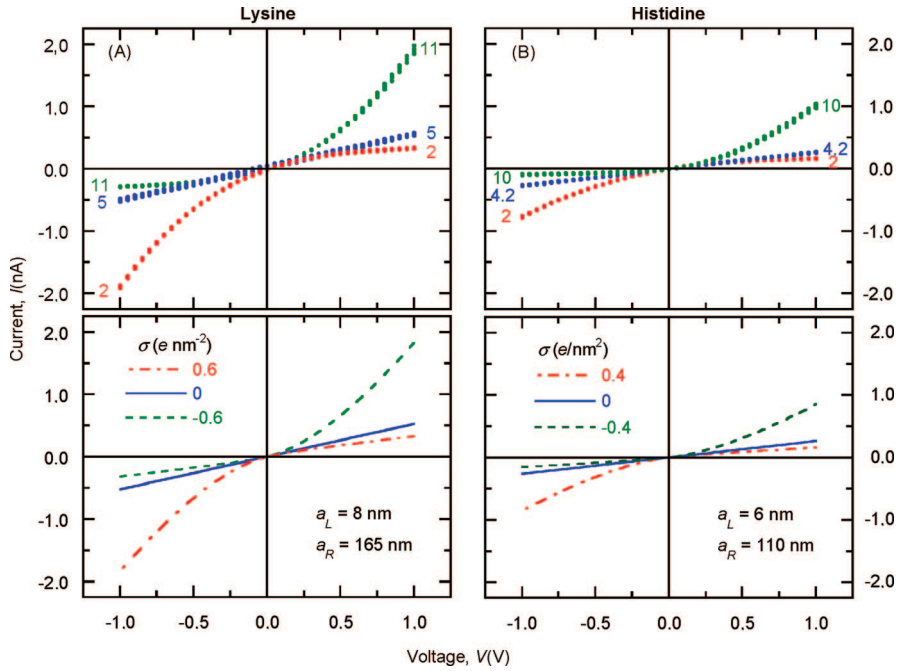

Figure 5. (A) Experimental *I*−*V* curves of the amphoteric nanopore (lysine) at pH = 2, 5, and 11 (up) and theoretical results from a PNP model (down). (B) Experimental *I*−*V* curves of the amphoteric nanopore (histidine) at pH = 2, 4.2, and 10 (up) and theoretical results from a PNP model (down). The fitting procedure gives an uncertainty range of 10% for the estimated surface charge density and pore radius.

been calculated, the only free parameter of the PNP model is the surface charge σ (in elementary charges per square nanometer). We emphasize finally that the values of σ in Figure 5 are in good agreement with those found previously for negatively charged conical nanopores.[43]

CONCLUSIONS

In conclusion, the amphoteric chains functionalized on the conical nanopore surface form the basis of a nanofluidic diode allowing pH-tunable rectification properties. The results demonstrate that virtually any characteristics required in practical applications can be accomplished with the same device by simply changing the pH of the external solutions. The conical nanopore has a well-defined, controlled structural asymmetry, showing selectivity and rectification properties that are dictated by the nanometer-sized tip region. The intrinsic (geometric and electrostatic) asymmetries of the device permit one to implement different functions on a unique nanostructure.

MATERIALS AND METHODS

Polymer foils of polyethylene terephthalate (PET) (Hostaphan RN 12, Hoechst) of 12 μm thickness were irradiated at the linear accelerator UNILAC (GSI, Darmstadt) with single swift heavy ions (Pb, U, and Au) having an energy of 11.4 MeV per nucleon. *N*-(3-Dimethylaminopropyl)-*N*′-ethylcarbodiimide hydrochloride (EDC, 98%, Fluka), pentafluorophenol (PFP, 99+ %, Aldrich), L-lysine (98 + %, Fluka), L-histidine (99.5+ %, Sigma), and copper(II) chloride dihydrate (99%, Merck, Germany) were used as received for the chemical modification. The surfactant Dowfax* 2A1 (Dow Chemical) was used as received without further purification.

Single asymmetric conical nanopores were fabricated in the irradiated PET membranes using surfactant-controlled asymmetric track-etching.[47] First, the tracked polymer membranes were irradiated with soft UV light (UV source provides ~1.5 and 4 W m^{-2} of the electromagnetic power of wavelength in the ranges of 280−320 and 320−400 nm, respectively) for 35 h. Second, the foil was mounted between the two compartments of the conductivity cell, where it served as a dividing wall. The compartment adjoining the UV-sensitized side was filled with pure etchant (6 M NaOH), while the other one facing the non UV-treated side of the membrane was filled with a protecting solution containing 6 M NaOH and 0.04% (v/v) surfactant. The etching process was carried out at 60 °C. During etching, a potential of −1 V was applied across the membrane in order to monitor the current flowing through the nascent pore. The current remains zero as long as the pore is not yet etched through and, after the breakthrough, a continuous increase in the current was observed. The etching process was stopped when the current reached a certain value. The channel was washed first with 1 M HCl in order to quench the etchant, followed by rinsing with deionized water.

In order to block the α-amino and α-carboxylic groups, a solution of L-lysine (50 mM) was prepared in 60% aqueous ethanol (C_2H_5OH/H_2O, 6:4 by volume) and solid copper chloride (25 mM) was added slowly with continuous stirring. As a result, the blue colored Cu(II) chelate complex of L-lysine was prepared containing a free amino group at the terminus of the chain, as shown in reaction scheme (a) in Figure 1.

All chemical reactions were carried out in the conductivity cell used for etching of tracked polymer foils. The carboxylic (−COOH) groups generated on the pore surface during the track-etching process were modified by the following procedure. First, these groups were converted into pentafluorophenyl esters by using ethanolic solution of *N*-(3-dimethylaminopropyl)-*N*′-ethylcarbodiimide hydrochloride (EDC, 100 mM) and pentafluorophenol (PFP, 200 mM) for 1 h. Second, the amine-reactive PFP esters were covalently coupled with the ε-amino group of the copper complex of lysine overnight. After washing with distilled water, the modified pores were exposed to ethylenediaminetetraacetic acid (EDTA, 100 mM) for 2 h in order to remove the copper ions from the surface of the pore. Finally, the modified pore was washed with distilled water thoroughly. Functionalization of L-histidine on the pore surface was done by activation of carboxylic groups into PFP esters following the same procedure described for lysine. After activation, reactive esters were condensed with the α-amino groups of L-histidine (50 mM) solution prepared in 60% aqueous ethanol and allowed to react overnight at room temperature. Finally, the functionalized membranes were washed with distilled water several times.

The membranes with the lysine and histidine functionalized single nanopores were mounted between the two halves of the conductivity cell, and both halves of the cell were filled with 0.1 M KCl solution. The pH of the electrolyte was adjusted by dilute HCl or KOH solutions. A Ag/AgCl electrode was placed into each half-cell solution, and a picoammeter/voltage source (Keithley 6487, Keithley Instruments, Cleveland, OH) was used to apply the desired transmembrane potential. To measure the resulting ion current flowing through the nanopore, a scanning triangle voltage from −2 to +2 V on the tip side was applied (the base side of the pore remained connected to the ground electrode).

Acknowledgment. M.A. thanks HEC of Pakistan, on receiving partial financial support. P.R. and S.M. acknowledge the support from Ministry of Science and Innovation of Spain, *Program of Materials*, and FEDER. We acknowledge Drs. B. Yameen (MPIP) and O. Azzaroni (INIFTA) for fruitful and enlightening discussions about the use of zwitterionic groups.

REFERENCES AND NOTES

1. Siwy, Z.; Fuliński, A. Fabrication of a Synthetic Nanopore Ion Pump. *Phys. Rev. Lett.* **2002**, *89*, 198103.
2. Lee, S.; Zhang, Y. H.; White, H. S.; Harrell, C. C.; Martin, C. R. Electrophoretic Capture and Detection of Nanoparticles at the Opening of a Membrane Pore Using Scanning Electrochemical Microscopy. *Anal. Chem.* **2004**, *76*, 6108–6115.
3. Lebedev, K.; Mafé, S.; Stroeve, P. Modeling Electrochemical Deposition Inside Nanotubes to Obtain Metal−Semiconductor Multiscale Nanocables or Conical Nanopores. *J. Phys. Chem. B* **2005**, *109*, 14523.
4. Zhang, Y. H.; Zhang, B.; White, H. S. Electrochemistry of Nanopore Electrodes in Low Ionic Strength Solutions. *J. Phys. Chem. B* **2006**, *110*, 1768–1774.
5. Umehara, S.; Pourmand, N.; Webb, C. D.; Davis, R. W.; Yasuda, K.; Karhanek, M. Current Rectification with Poly-L-Lysine-Coated Quartz Nanopipettes. *Nano Lett.* **2006**, *6*, 2486–2492.
6. Wharton, J. E.; Jin, P.; Sexton, L. T.; Horne, L. P.; Sherrill, S. A.; Mino, W. K.; Martin, C. R. A Method for Reproducibly Preparing Synthetic Nanopores for Resistive-Pulse Biosensors. *Small* **2007**, *3*, 1424–1430.
7. Dekker, C. Solid-State Nanopores. *Nat. Nanotechnol.* **2007**, *2*, 209–215.
8. Ku, J. R.; Lai, S. M.; Ileri, N.; Ramírez, P.; Mafé, S.; Stroeve, P. pH and Ionic Strength Effects on Amino Acid Transport through Au-Nanotubule Membranes Charged with Self-Assembled Monolayers. *J. Phys. Chem. C* **2007**, *111*, 2965–2973.
9. Schoch, R. B.; Han, J.; Renaud, P. Transport Phenomena in Nanofluidics. *Rev. Mod. Phys.* **2008**, *80*, 839–883.

10. Griffiths, J. The Realm of the Nanopore. *Anal. Chem.* **2008**, *80*, 23–27.
11. Ali, M.; Yameen, B.; Neumann, R.; Ensinger, W.; Knoll, W.; Azzaroni, O. Biosensing and Supramolecular Bioconjugation in Single Conical Polymer Nanochannels. Facile Incorporation of Biorecognition Elements into Nanoconfined Geometries. *J. Am. Chem. Soc.* **2008**, *130*, 16351–16357.
12. Martin, C. R.; Siwy, Z. S. Learning Nature's Way: Biosensing with Synthetic Nanopores. *Science* **2007**, *317*, 331–332.
13. Healy, K.; Schiedt, B.; Morrison, A. P. Solid-State Nanopore Technologies for Nanopore-Based DNA Analysis. *Nanomedicine* **2007**, *2*, 875–897.
14. Cervera, J.; Schiedt, B.; Neumann, R.; Mafé, S.; Ramírez, P. Ionic Conduction, Rectification, and Selectivity in Single Conical Nanopores. *J. Chem. Phys.* **2006**, *124*, 104706.
15. Mafé, S.; Manzanares, J. A.; Pellicer, J. On the Introduction of the Pore Wall Charge in the Space-Charge Model for Microporous Membranes. *J. Membr. Sci.* **1990**, *51*, 161–168.
16. Ali, M.; Schiedt, B.; Healy, K.; Neumann, R.; Ensinger, W. Modifying the Surface Charge of Single Track-Etched Conical Nanopores in Polyimide. *Nanotechnology* **2008**, *19*, 085713.
17. Alcaraz, A.; Ramirez, P.; Garcia-Gimenez, E.; López, M. L.; Andrio, A.; Aguilella, V. M. A pH-Tunable Nanofluidic Diode: Electrochemical Rectification in a Reconstituted Single Ion Channel. *J. Phys. Chem. B* **2006**, *110*, 21205–21209.
18. Nishizawa, M.; Menon, V. P.; Martin, C. R. Metal Nanotubule Membranes with Electrochemically Switchable Ion-Transport Selectivity. *Science* **1995**, *268*, 700–702.
19. Chun, K.-Y.; Mafé, S.; Ramírez, P.; Stroeve, P. Protein Transport through Gold-Coated, Charged Nanopores: Effects of Applied Voltage. *Chem. Phys. Lett.* **2006**, *418*, 561–564.
20. English, A. E.; Mafé, S.; Manzanares, J. A.; Yu, X.; Grosberg, A. Y.; Tanaka, T. Equilibrium Swelling Properties of Polyampholytic Hydrogels. *J. Chem. Phys.* **1996**, *104*, 8713–8720.
21. Mafé, S.; Manzanares, J. A.; English, A. E.; Tanaka, T. Multiple Phases in Ionic Copolymer Gels. *Phys. Rev. Lett.* **1997**, *78*, 3086–3089.
22. Ramírez, P.; Mafé, S.; Tanioka, A.; Saito, K. Modelling of Membrane Potential and Ionic Flux in Weak Amphoteric Polymer Membranes. *Polymer* **1997**, *38*, 4931–4934.
23. Jimbo, T.; Ramírez, P.; Tanioka, A.; Mafé, S.; Minoura, N. Passive Transport of Ionic Drugs through Membranes with pH-Dependent Fixed Charges. *J. Colloid Interface Sci.* **2000**, *225*, 447–454.
24. Matsumoto, H.; Koyama, Y.; Tanioka, A. Characterization of Novel Weak Amphoteric Charged Membranes Using Zeta-Potential Measurements. Effect of Dipolar Ion Structure. *Langmuir* **2001**, *17*, 3375–3381.
25. Siwy, Z.; Heins, E.; Harrell, C. C.; Kohli, P.; Martin, C. R. Conical−Nanotube Ion−Current Rectifiers: The Role of Surface Charge. *J. Am. Chem. Soc.* **2004**, *126*, 10850–10851.
26. Vlassiouk, I.; Siwy, Z. Nanofluidic Diode. *Nano Lett.* **2007**, *7*, 552–556.
27. Gracheva, M. E.; Vidal, J.; Leburton, J.-P. p−n Semiconductor Membrane for Electrically Tunable Ion Current Rectification and Filtering. *Nano Lett.* **2007**, *7*, 1717–1722.
28. Karnik, R.; Duan, C.; Castelino, K.; Daiguji, H.; Majumdar, A. Rectification of Ionic Current in a Nanofluidic Diode. *Nano Lett.* **2007**, *7*, 547–551.
29. Karnik, R.; Fan, R.; Yue, M.; Li, D.; Yang, P.; Majumdar, A. Electrostatic Control of Ions and Molecules in Nanofluidic Transistors. *Nano Lett.* **2005**, *5*, 943–948.
30. Kalman, E. B.; Vlassiouk, I.; Siwy, Z. Nanofluidic Bipolar Transistors. *Adv. Mater.* **2008**, *20*, 293–297.
31. Spohr, R. Status of Ion Track Technology−Prospects of Single Tracks. *Radiat. Meas.* **2005**, *40*, 191–202.
32. Apel, P. Y.; Blonskaya, I. V.; Dmitriev, S. N.; Orelovitch, O. L.; Presz, A.; Sartowska, B. A. Fabrication of Nanopores in Polymer Foils with Surfactant-Controlled Longitudinal Profiles. *Nanotechnology* **2007**, *18*, 305302.
33. Cornelius, T. W.; Apel, P. Y.; Schiedt, B.; Trautmann, C.; Toimil-Molares, M. E.; Karim, S.; Neumann, R. Investigation of Nanopore Evolution in Ion Track-Etched Polycarbonate Membranes. *Nucl. Instrum. Methods Phys. Res. B* **2007**, *265*, 553–557.
34. Ramírez, P.; Apel, P. Y.; Cervera, J.; Mafé, S. Pore Structure and Function of Synthetic Nanopores with Fixed Charges: Tip Shape and Rectification Properties. *Nanotechnology* **2008**, *19*, 315707.
35. Wolf, D. E.; Valiant, J.; Peck, R. L.; Folkers, K. Synthesis of Biocytin. *J. Am. Chem. Soc.* **1952**, *74*, 2002–2003.
36. Kuwata, S.; Watanabe, H. Removal of Copper from Copper Complex of Omega-Acylamino Acid with EDTA. *Bull. Chem. Soc. Jpn.* **1965**, *38*, 676–677.
37. Mathews, C. K.; van Holde, K. E. *Biochemistry*; Benjamin/Cummings: Redwood City, CA, 1990.
38. Hermanson, G. T. *Bioconjugate Techniques*; Academic Press: San Diego, CA, 1996.
39. Cervera, J.; Schiedt, B.; Ramírez, P. A Poisson/Nernst-Planck Model for Ionic Transport Through Synthetic Conical Nanopores. *Europhys. Lett.* **2005**, *71*, 35–41.
40. Sexton, L. T.; Horne, L. P.; Martin, C. R. Developing Synthetic Conical Nanopores for Biosensing Applications. *Mol. BioSyst.* **2007**, *3*, 667–685.
41. Ramírez, P.; Mafé, S.; Alcaraz, A.; Cervera, J. Modeling of pH-Switchable Ion Transport and Selectivity in Nanopore Membranes with Fixed Charges. *J. Phys. Chem. B* **2003**, *107*, 13178–13187.
42. Ramírez, P.; Mafé, S.; Aguilella, V. M.; Alcaraz, A. Synthetic Nanopores with Fixed Charges: An Electrodiffusion Model for Ionic Transport. *Phys. Rev. E* **2003**, *68*, 011910.
43. Cervera, J.; Alcaraz, A.; Schiedt, B.; Neumann, R.; Ramírez, P. Asymmetric Selectivity of Synthetic Conical Nanopores Probed by Reversal Potential Measurements. *J. Phys. Chem. C* **2007**, *111*, 12265–12273.
44. Ramírez, P.; Gómez, V.; Cervera, J.; Schiedt, B.; Mafé, S. Ion Transport and Selectivity in Nanopores with Spatially Inhomogeneous Fixed Charge Distributions. *J. Chem. Phys.* **2007**, *126*, 194703.
45. Constantin, D.; Siwy, Z. S. Poisson−Nernst−Planck Model of Ion Current Rectification through a Nanofluidic Diode. *Phys. Rev. E* **2007**, *76*, 041202.
46. Gracheva, M. E.; Leburton, J. P. Electrolytic Charge Inversion at the Liquid−Solid Interface in a Nanopore in a Doped Semiconductor Membrane. *Nanotechnology* **2007**, *18*, 145704.
47. Ali, M.; Bayer, V.; Schiedt, B.; Neumann, R.; Ensinger, W. Fabrication and Functionalization of Single Asymmetric Nanochannels for Electrostatic/Hydrophobic Association of Protein Molecules. *Nanotechnology* **2008**, *19*, 485711.